

Characterization of H2M monolithic pixel sensor ASIC

Milica Rajčić

Under the supervision of Younes Otarić and Philipp Gadow

CERN, Geneva, Switzerland

Abstract

Monolithic active pixel detectors are a promising technology for vertex and tracking detectors in potential future lepton colliders. In particular, the advanced 65nm CMOS imaging technology offers higher density and reduced power consumption compared to previous approaches. This report will cover the process of testing a monolithic silicon pixel detector under development, named H2M (Hybrid-to-Monolithic), that will potentially constitute trackers of future lepton colliders. Laboratory and test-beam measurements were carried out. Preliminary results of a thinned sample ($30\mu m$) of the H2M detector are presented in this report.

Keywords

monolithic silicon pixel detectors; H2M; future colliders.

1 Introduction to silicon detectors

Silicon pixel detectors play a crucial role in high-energy physics, in terms of advancing and understanding the fundamental structure of matter. Silicon tracking detectors are responsible for identifying trajectories of charged particles produced in high-energy collisions, such as those occurring in accelerators like the *Large Hadron Collider (LHC)*.

The essence of silicon detectors lies in their exceptional spatial resolution, fast response times and the ability to operate in high radiation environments. These are the core characteristics that future accelerators, like the *Future Circular Collider (FCC-ee)* and the *Compact Linear Collider (CLIC)*, will use to accurately track particle trajectories, distinguish different types of particles and detect rare events. As particle physicists dig deeper, silicon detectors play a crucial role in testing new theories, discovering novel particles and pushing the boundaries of our knowledge even further.

1.1 Working principle

A silicon pixel detector consists of an array of $p-n$ junctions. It is operated in reverse bias mode to deplete the silicon bulk of free charge carriers, responsible for creating an electric field between the sensor backside and readout electrodes.

The width of the depletion zone, ω , depends on the applied reverse bias voltage, V_{bias} , and on the effective doping concentration of the sensor, N , according to the formula:

$$\omega \approx \sqrt{\frac{2\varepsilon}{qN} V_{bias}},$$

where q is the elementary charge and $\varepsilon = 11.68 \times 8.854 \times 10^{-12} F \cdot m^{-1}$ is the permittivity of silicon. To maximize the ionization signals originating from traversing particles, the sensor should be operated at a bias voltage equal to or greater than the full-depletion voltage, V_{dep} , which corresponds to the voltage necessary to deplete the entire thickness of the sensor, d :

$$V_{dep} = \frac{qNd^2}{2\varepsilon}.$$

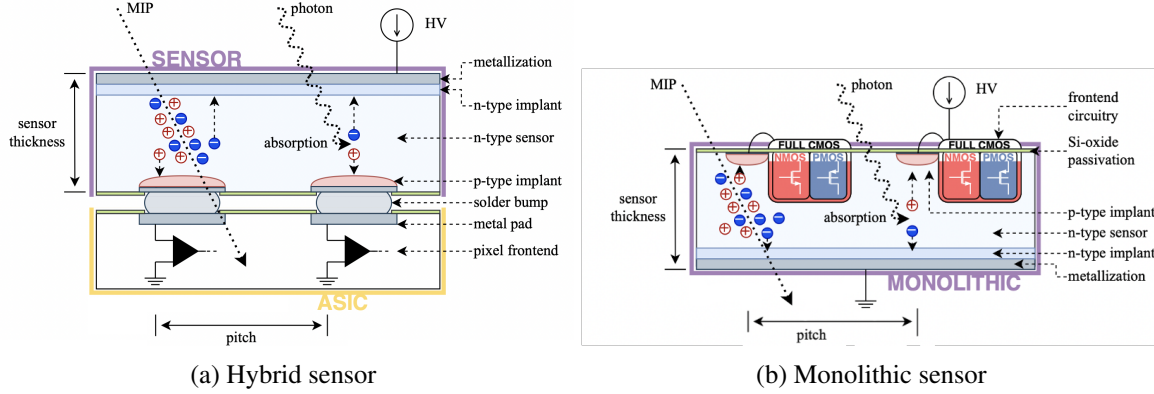


Figure 1: Schematic cross-sections of a hybrid and monolithic pixel detectors, respectively, along with signal generation in cases of traversing MIP and photon are displayed

1.2 Hybrid and monolithic silicon pixel detectors

Taking into account integration and construction of the sensor and readout electronics, we differentiate between two types of silicon pixel detectors: *hybrid* and *monolithic* silicon pixel detectors. Each type comes with its own structure and advantages.

Hybrid silicon pixel detectors, introduced in Figure 1a, have the sensor and readout ASIC (Application Specific Integrated Circuit) fabricated on separate silicon wafers and connected via bump bonding. Inside a sensor, charges are generated by traversing particles due to ionisation. Free charges being present in the electrical field are drifting towards the electrodes thus contributing to signal creation. The fact that the sensor and readout electronics are separated, allows for them to be individually optimized, which may improve performance of the detector. However, the assembly is complex due to the need for precise alignment and bonding of separate layers, which increases the material budget of the final product. The consequences are relatively high costs and manufacturing challenges. They are widely used in large-scale experiments (ie. ATLAS, CMS) due to their reliability and high performance, but for usage in high-energy physics, where thin layers of detectors are needed to avoid scattering and absorption of particles, hybrid silicon detectors can not be manufactured thin enough.

Monolithic silicon pixel detectors, on the other side, have integrated both the sensor and readout electronics on a single silicon chip (Figure 1b). This means that charge collection and signal processing are taking place in the same wafer. Sensor and readout electronics integration results in lower material consumption, simplified manufacturing process and reduced thickness compared to hybrid silicon detectors. In the same time, integration means that both parts of the detector are fabricated using the same technique on a common substrate, and this, usually, leads to certain constraints in terms of design optimization. From the complexity angle, these detectors are simple and do not require bonding, which makes them suitable for a variety of applications. Their most important characteristic, in terms of this research, is that they are compact and thin, which makes them advantageous in environments where minimizing the detector's physical footprint is important.

The purpose of this research is to examine one type of high-energy particle detectors that will be used in trackers of future colliders. New particles, along with the existing ones, are aimed to be detected, which sets new standards for developing detectors. High-precision and cost-effective large-scale fabrication are desired detector's characteristics. The integrity of monolithic silicon pixel detectors paves them the way to be the constituent of experiments at future colliders.

2 Hybrid-to-Monolithic (H2M) silicon pixel test chip

The H2M is a monolithic silicon pixel detector that explores design choices and new technology approaches which will find its purpose in future electron-positron collider facilities. It is a descendant of a well known hybrid detector whose architecture was ported into a chip using 65nm CMOS imaging process. The detector is a square pixel matrix of size 64×16 , with $35\mu\text{m}$ pitch for a total sensitive area of $2.24 \times 0.56\text{mm}^2$. Each pixel consists of a collection electrode, analog front-end and digital logic. Figure 2 shows a block diagram of the H2M. More on the structure of the detector can be found in H2M reference manual [1].

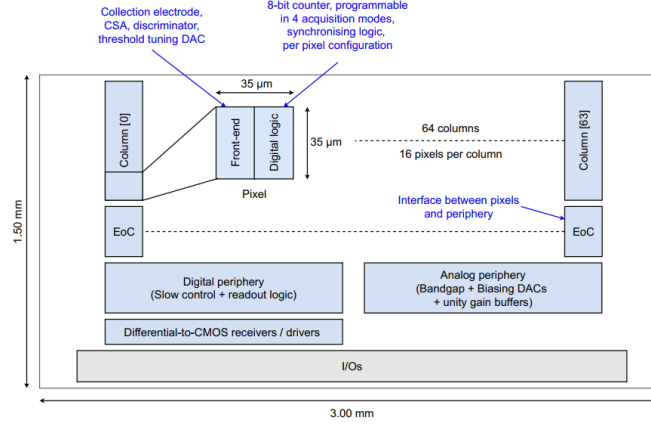


Figure 2: Block diagram of the H2M chip

So far, there are two versions of H2M detectors available and they only differ in their thickness: $50\mu\text{m}$ and $30\mu\text{m}$ thick detectors. Out of entire detector thickness, $10\mu\text{m}$ is the sensitive area responsible for particle detection, and the rest goes to electronics metal stack and the substrate.

The main focus of this report is to provide an overview of the results obtained on thin H2M detectors ($30\mu\text{m}$ thin H2M-6 and H2M-7) available at CERN. The motivation was to examine their behaviour in laboratory and test-beam environments and conclude about their functionality.

3 Overview of the work

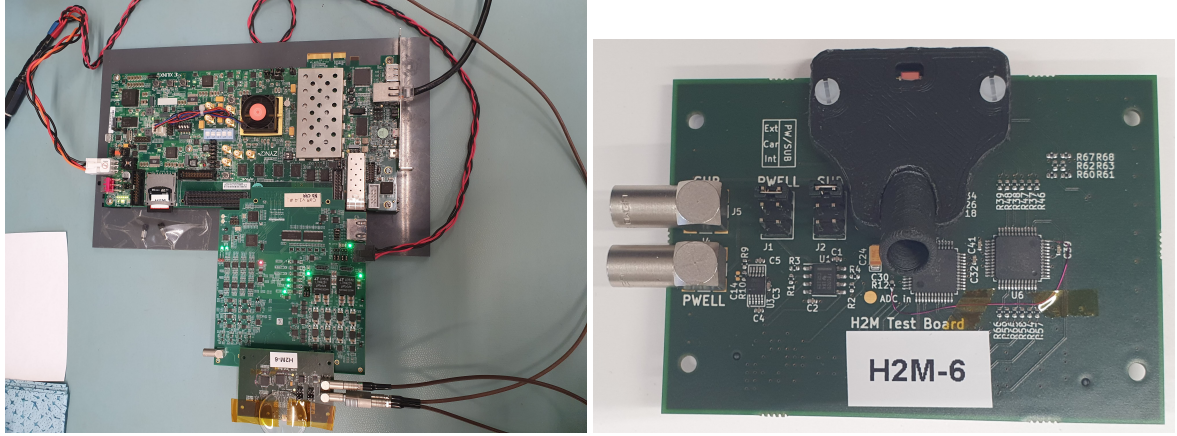
The focus of this research was to study the functionality of $30\mu\text{m}$ thick detectors (H2M-6 and H2M-7), both, in laboratory and in test-beam. For comparison, existing results for a $50\mu\text{m}$ thick sample (H2M-4) will be included. The measurements are taken for different values of bias voltage (-1.2V , -3.6V , -4.2V and -4.8V) for comparison purposes.

4 Lab measurements

The first step in characterizing this detector is taking place in one of the labs at CERN, where the setup for taking measurements is assembled (Figure 3a). Constituents of the assembly are the detector, H2M-6 in this case, and a test system, called *Caribou*.

Caribou is a versatile test system developed by CERN and collaborating institutes and used for prototyping and testing of silicon detectors. There are three core components of the system: Chip board, CaR board and a System-on-chip (SoC) board. Also, it uses *Peary* as a data acquisition software. For more on *Caribou* see Ref [2].

Figure 3b shows the H2M-6 detector mounted on a dedicated chip board and protected with a 3D printed cover. On terminals on the left bias voltage can be applied to deplete the sensor. First of all,



(a) Laboratory setup that consists of DAQ system (Caribou) and H2M-6 detector (b) H2M-6 detector, protected with 3D cover, connected to the Chip board

Figure 3

the detector is tested without a particle source to characterize and calibrate the pixel matrix. That is done in order to extract the single-pixel noise (the amount of noise (in electrons) that every pixel inputs into the system) and this value is aimed to be minimized. The steps taken to accomplish laboratory characterization are the following: threshold equalization, single-pixel noise measurement and charge calibration. The entire procedure from the laboratory will be presented in detail in the next few pages.

4.1 Threshold equalization

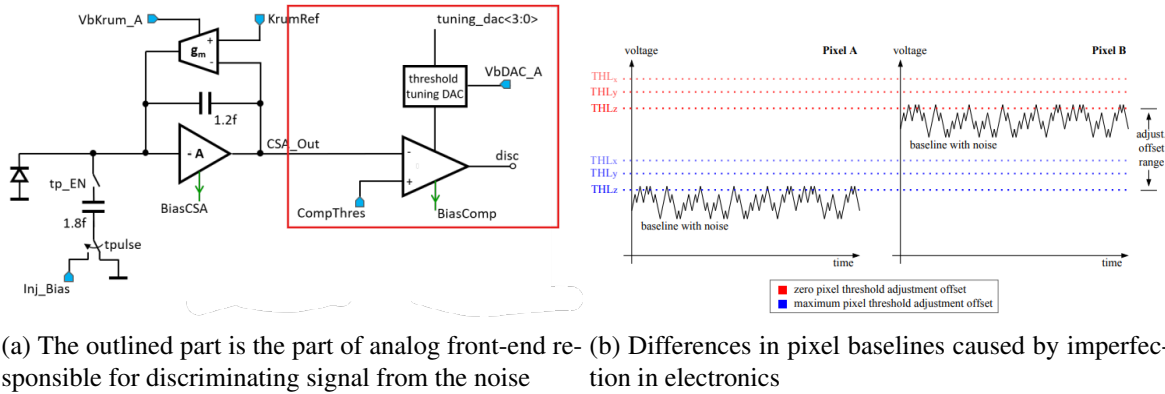
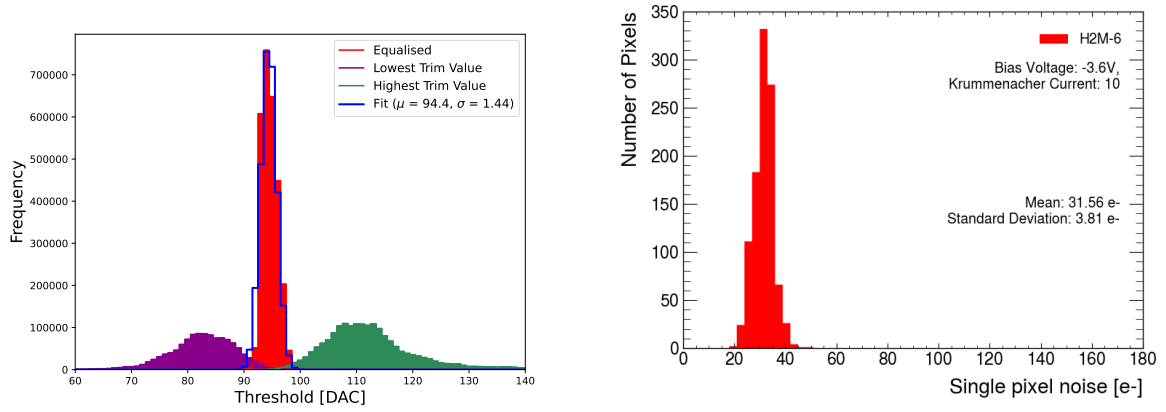


Figure 4

The outlined section of the Figure 4a represents the comparator responsible for separation of good signal from noise. The signal is compared with a globally provided threshold *CompThres*, controlled by an 8-bit DAC (Digital-to-Analog Converter). The value of the threshold should be set high enough so that no noise passes the comparator and, at the same time, low enough so that it is ensured that valuable signal passes it. But, there is one difficulty that makes this comparison complex due to process variations of the pixel readout electronics. This divergence leads to small fluctuations of baselines for different pixels, as depicted on the Figure 4b. Due to baseline variations and the fact that the threshold value is unique for all pixels, it may happen that either noise passes the comparator, either good signal does not pass it. The solution for this is to homogenize detection across entire matrix, which is done by equalizing

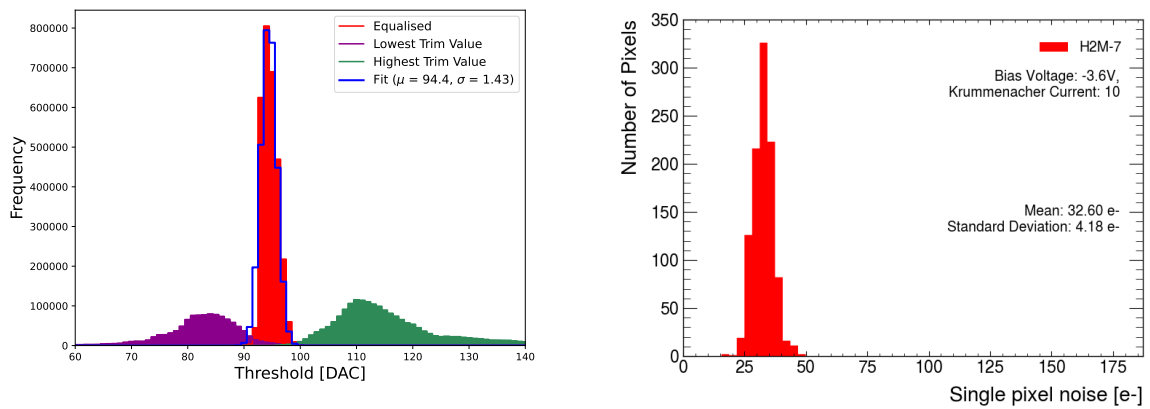
the threshold.

The equalization process uses a 4-bit tuning DAC to locally tune the threshold in a range of 16 unit steps. For each step, a threshold scan is done for all pixels. It allows to reconstruct S-curves for each pixel. The latter shows the number of pixel counts as a function of threshold. The baseline position of every pixel is then extracted as the mean of the corresponding S-curve derivative, and the noise as the standard deviation. After repeating the same procedure for all pixels and all tuning DAC settings, the baseline and noise distribution of all pixels are obtained. Figure 5a shows summary plots of the equalization procedure. The baseline distributions for the lowest and highest *Tuning DAC* values for all pixels are plotted. A target baseline is then chosen as the average of the two distribution peaks and the individual pixels are tuned accordingly. Their distribution is represented by the red curve on the Figure 5a. Mean baseline value for the detector is obtained ($\mu = 94.4 DAC$) from the fit, while the width of it represents the dispersion of all pixel baselines.



(a) Threshold equalization of whole matrix for H2M-6 with $V_{bias} = -3.6V$ (b) Distribution of single-pixel noise across the whole matrix of H2M-6 with $V_{bias} = -3.6V$

Figure 5



(a) Threshold equalization for H2M-7 with $V_{bias} = -3.6V$ (b) Single-pixel noise for H2M-7 with $V_{bias} = -3.6V$

Figure 6

Also, Figure 6 shows plots obtained of threshold equalization and single-pixel noise for H2M-7. When compared with the corresponding H2M-6 plots, one can notice similar results.

4.2 Single-pixel noise

On the other hand, from the width of the S-curve derivative single-pixel noise is extracted. Figure 5b shows the single-pixel noise plot. In other words, not all pixels input the same amount of noise into measurements. To get to know how noisy the pixels are, we plotted the single-pixel noise distribution across the whole matrix. Ideally, there is no noise, but in reality this is not the case and that is why the key is to have the as low noise as possible. From the peak of the curve we conclude the average single-pixel noise value. Figure 5b and Figure 6b suggest that both detectors H2M-6 and H2M-7 yield around the same matrix noise. And from the width of the distribution of the single-pixel noise, which is pretty narrow, it can be said that noise is rather homogeneous across the matrix.

4.3 Charge calibration

Results obtained from threshold equalization and single-pixel noise are all in units of DACs which is not convenient in the world of particle physics where the elementary unit is e^- , the number of electron-hole pairs created in the sensor. From measurements expressed in units of e^- , conclusions are simply drawn, and this determines the last step for laboratory measurements.



Figure 7: Laboratory setup for charge calibration with Fe-55, a radioactive source of photons with the fixed energy of 5.9keV

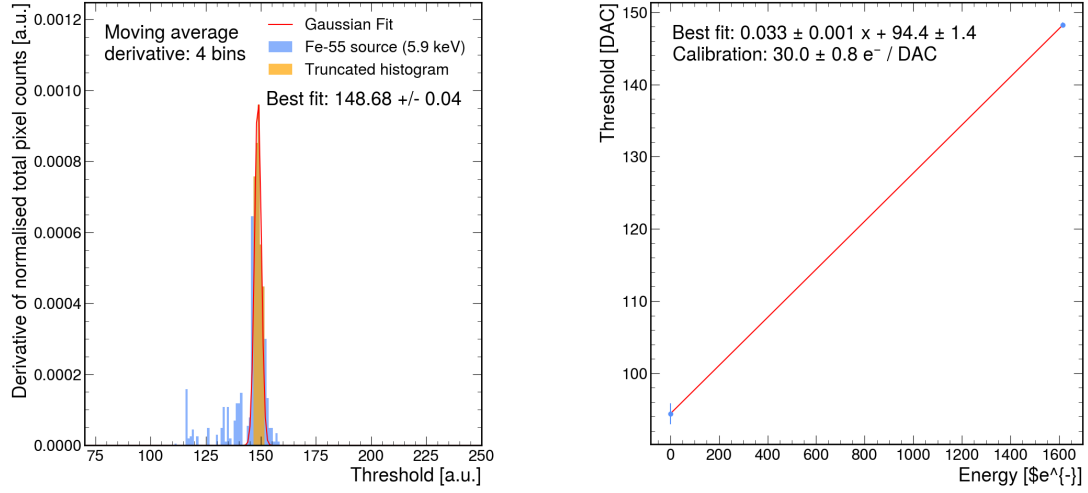
Figure 7 shows the same laboratory assembly with the addition of the metal box which stores and protects a radioactive source Fe-55 with a peak Alpha (photon) emission at 5.9keV. The source is set up on a source holder directly above the detector and everything is ready for taking measurements.

When a particle is spontaneously emitted by the radioactive source, the sensor is able to detect it due to the particle's interaction with the sensitive material. In this case, a photon is hitting silicon and being fully absorbed in the depletion region of the sensor which leads to creation of electron/hole pairs that form a signal on electrodes. Having on mind that the energy required to produce an electron/hole pair in silicon is 3.62eV, and a photon hitting sensor has energy of 5.9keV, simple calculation indicates that *one photon produces 1630 electron/hole pairs*.

With the radioactive source in place, the exact same procedure is being done as without a source. Threshold scan is executed for determining threshold value for which the most of pixels are firing, which means that they detect a signal from the source. From the measured data, a curve is obtained with a photon peak that is shown on Figure 8a. For the threshold value with the most pixel firing a peak is present. In order to determine it the bin number is set in software that acts like a window function that scans a range determined by the bin variable throughout threshold axis and looks for a peak in it. When the peak is detected it is fitted into a Gaussian with the mean representing the best threshold for detecting

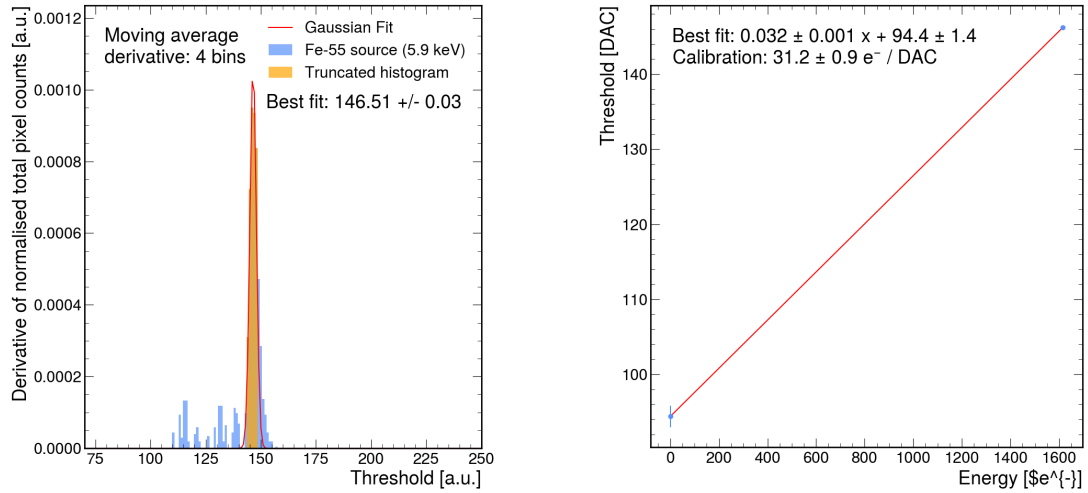
a photon (Figure 8a shows it is 148.68 DAC).

Now, results with and without source can be combined to obtain a relation between e^- and DAC. It is a linear fit on Figure 8b that is acquired by connecting two points from two measurements. First point, the lower one, is from the measurement without a source. On the other hand, the upper point is obtained from the iron source measurement where at threshold of 148.68 DAC, a photon is releasing $1620e^-$. Charge calibration for this sensor is acquired from the slope of the linear fit, and in this case 1 DAC corresponds to $30.0e^-$. Similarly, calibration plots for H2M-7 shown of Figure 9 are similar to the ones for H2M-6. One thing that should be noted for H2M-7 is that 1 DAC corresponds to $31.2e^-$.



(a) Threshold scan with iron source. The peak says (b) Charge calibration linear fit for H2M-6 with $V_{bias} = -3.6V$ about the energy of the source

Figure 8



(a) Threshold scan with iron source (H2M-7) (b) Charge calibration for H2M-7 with $V_{bias} = -3.6V$

Figure 9

5 Test-beam measurements

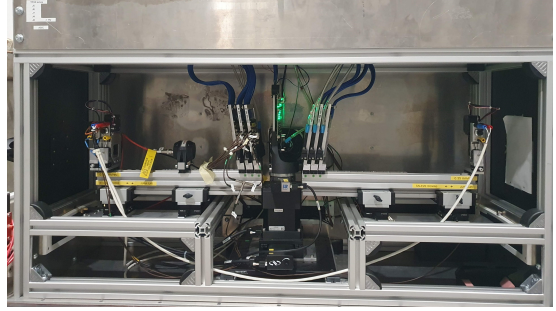
For further testing of the H2M detectors there are test-beams. In the test-beam facility the detector is exposed to a beam of high-energy particles in order to study the detection performance [3]. In test-beam facilities, high-energy particles are provided to hit the sensor. Unlike low-energy photons in the laboratory, these particles ionise silicon as they penetrate it creating an electron/hole pair per ion. This secures a larger signal compared to the one from the laboratory measurements.

The test-beam measurements took place in the experimental hall in the north area with a secondary beam provided by the *SPS* (*Super Proton Synchrotron*). *SPS* is the second-largest accelerator at CERN, situated on CERN's French side, in Preveessin. While *SPS* has historically handled multiple types of particles, today it only operates with protons from *Proton Synchrotron* (*PS*). It accelerates them and provides beams up to 450GeV for the LHC, the NA61/SHINE and NA62 and the COMPASS experiments [5]. Figure 10a shows the north-area test-beam hall where beams are delivered by the *SPS*. More information about its historical accomplishments can be found in this article [4].

Figure 10b shows how the setup for the test-beam measurements for the H2M-6 in the *SPS* looked like. It was located in the H6 beam line supplied with 120GeV charged pion beam passing through the setup. The H2M detector is situated in the middle of the setup. There are three reference detectors in front of the detector and also three behind it that are called *Timepix3 reference telescope*. The telescope is used for accurate tracking of particles and reconstruction of their tracks which is farther used in test-beam analysis.



(a) CERN North Area H6 beam line



(b) Test-beam setup

Figure 10

For test-beam data reconstruction a dedicated software, called *corrvreckan* was used [6]. This handy tool simplified the steps of aligning our system and reconstructing tracks for the data analysis and production of performance results.

5.1 Alignment and track reconstruction

The first thing that was needed to be looked at after collecting the data from test-beam was prealignment files for both, the *Timepix3* telescope and the H2M. These files contain coordinates for every plane in our setup. Having their positions correctly stored is crucial for accurate detection and reconstruction of particle tracks. Since the coordinates in these files are not written down precisely enough, software alignment is mandatory to be done.

The alignment process was done in three steps. For each step the window in which a hit should be detected gets smaller. If a hit is inside the window the track should be reconstructed. According to this, planes are being moved up, down or rotated in order to adjust hit points to create a straight line. Repeating this process with smaller windows, assures that the particle hits in the H2M are properly associated with the ones belonging to tracks in the telescope.

Tracking particles is done using the six reference detectors surrounding the H2M-6. When they are well aligned, particles crossing their planes leave traces in forms of hits that are reconstructed as a straight line. The latter is what is referred to as a particle track.

5.2 Association of hits to tracks

After good alignment, the particle hits detected by the H2M can be associated to the reconstructed tracks in the telescope. This is where the detector is showing its functionality, by determining its ability to detect a particle already detected by telescope detectors and belonging to a reconstructed track. Particle hits on the H2M detector can be associated with a track if it is detected inside a window around a track. Otherwise, if the hit is not associated with any of the reconstructed tracks, it is a fake hit.

5.3 Efficiency of the detector

Efficiency of the detector is a measurement that assesses the performance of the detector in detecting traversing particles. Its definition is presented below and is computed for different threshold values:

$$E_{ff} = \frac{N_{tracks_associated_with_hits_on_H2M}}{N_{total_tracks}}$$

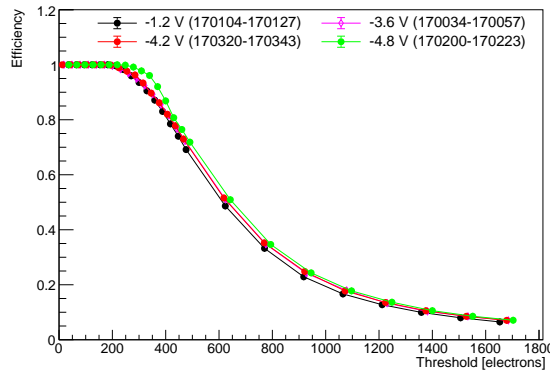


Figure 11: Efficiency plot taken for different bias voltage values for H2M-6

Figure 11 shows efficiency as a function of threshold for different values of bias voltage. For higher bias voltages the depletion region of the silicon detector gets wider and, therefore, higher efficiency is expected compared to the lower ones. From the efficiency curves, it can be noticed that, if we increase the bias voltage, the efficiency gets higher for higher threshold values. This is in accordance with our expectations. For nominal threshold of 103 DAC efficiency is above 98%. Also, from certain values of threshold the curve starts falling which means that signal is under the threshold value. Therefore, the number of hits on the detector begins to fall towards the efficiency of zero. For good functionality, as high value of efficiency as possible is desired because the aim is to have a high percentage of hits that belong to reconstructed tracks. The nominal threshold value is determined so that it has high enough efficiency and is above the noise. When we look at the Figure 13, we see that for higher thresholds not all pixels have the same efficiency. This is the reason why for the nominal threshold efficiency is not 100%. Also, when we decrease the threshold, efficiency reaches 100%, but since these threshold values are close to the baseline, where the signal is corrupted by noise, we start getting more fake hits.

5.4 Fake-hit rate of the detector

Efficiency alone is not enough to look at, but in addition of fake-hit rate graph it gives more valuable results. All the hits on the detector that do not belong to any of the reconstructed tracks contribute to

fake-hit rate. Figure 12 shows how fake-hit rate changes depending on the bias voltage. Looking at it, one can say that the fake-hit rate becomes higher with the threshold approaching to the baseline where the signal is affected by noise. From the plot, fake-hit rate curve for $V_{bias} = -3.6V$ is below the curve for $V_{bias} = -4.8V$. This curve has a high plateau for low thresholds which indicates that there is a lot of noise passing over the threshold. The sudden fall begins for threshold close to the baseline and, finally, there is an almost constant trend suggesting a very low fake-hit multiplicity.

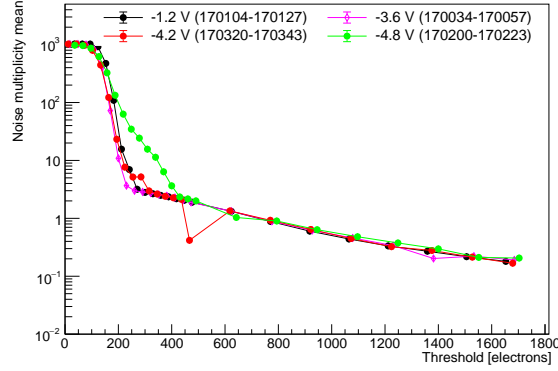


Figure 12: Fake-hit rate plot taken for different bias voltage values for H2M-6

When both, efficiency and fake-hit rate, curves are taken into account one is interested in determining the threshold range with high efficiency and low fake-hit rate in the same time. Setting up threshold that belongs to this range is the optimal option. Moreover, bias voltage is another parameter that affects threshold optimization.

An important aspect that impacts the way the detector works is the presence of the readout electronics on chip. For the H2M detector this is a huge challenge because of experiencing uneven detection throughout a pixel (Figure 13), which is the reason for lower efficiencies at higher thresholds. For low thresholds efficiency seems homogeneous throughout the matrix, but this is due to the high fake-hit multiplicity. Only when we take a look at higher thresholds the pixel inefficiency is visible. From the graphs, it is clear that the area where the readout electronics are located is where the in-pixel inefficiency is the highest, which is on the edges of the detector. This phenomenon has to be taken into account when determining the nominal threshold and is crucial for further research and development of the H2M.

6 Conclusions

The work done on characterization of the thin ($30\mu m$) H2M detectors comes up with promising results but also with a space for their improvement. Laboratory measurements (for H2M-6 and H2M-7) show quite good equalization result with narrow dispersion. The same stands for single-pixel noise which is $\sim 31e^-$ (H2M-6) and $\sim 33e^-$ (H2M-7) which is a satisfying result. Compared to the existing H2M-4 laboratory results, conclusion is that the thin detectors are, at least, as good as the thick one.

For test-beam results (H2M-6), efficiency and fake-hit rate plots are indicating that it is possible to obtain high efficiency while having decently low fake-hit rate which is encouraging starting point for further research and development of even thinner detectors.

Acknowledgements

I wish to thank CERN for providing me the remarkable opportunity to contribute to research taking place there, as well as to R&D group for helping me through my entire journey on this subject.

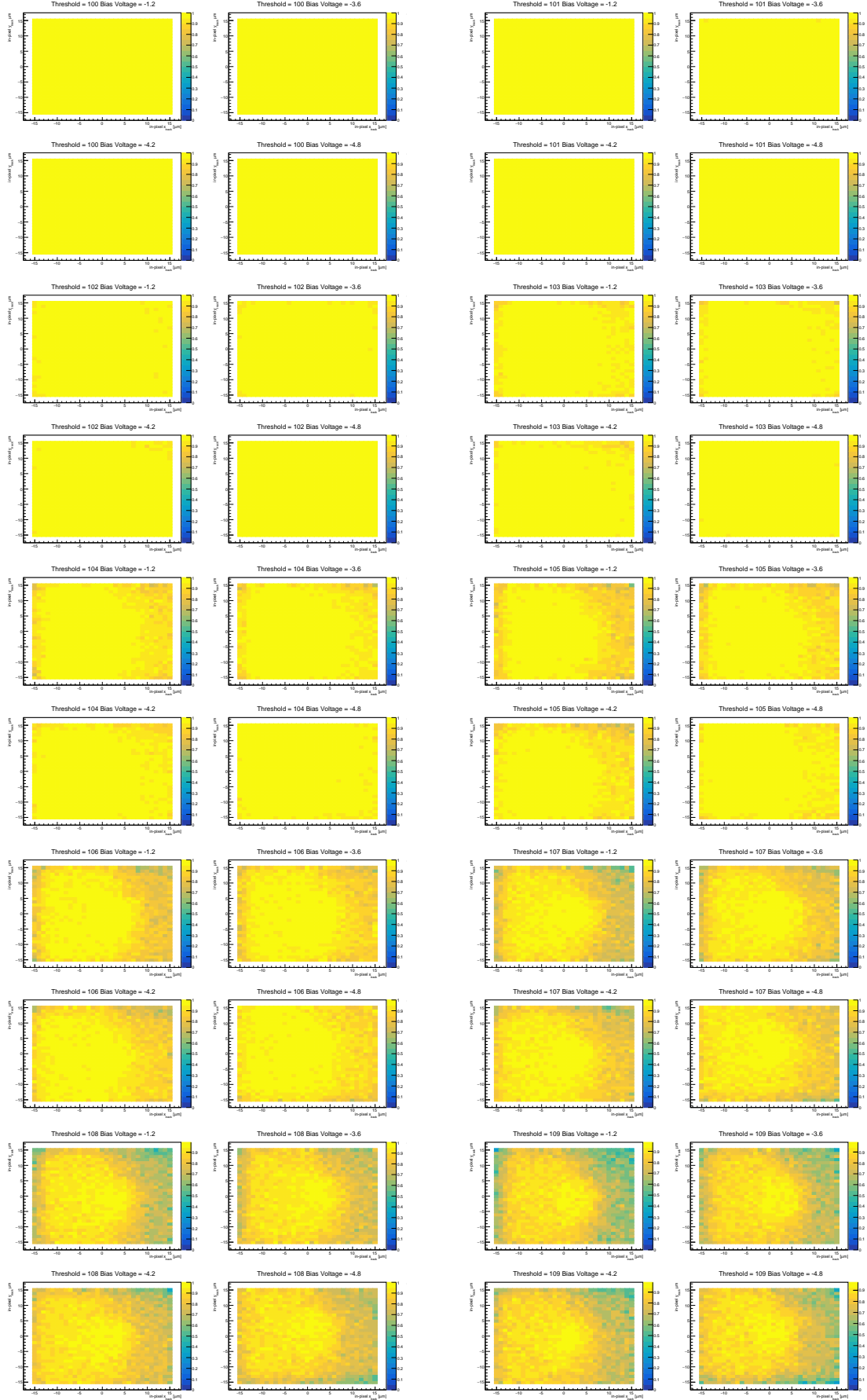


Figure 13: In-pixel efficiency heatmaps of H2M-6, plotted for $V_{bias} = -1.2V, -3.6V, -4.2V, -4.8V$ and threshold range from 100 DAC to 109 DAC

Bibliography

- [1] I. Kremastiotis, *H2M reference manual* (CERN EP-ESE-ME, 2023)
- [2] T. Vanat, *Caribou - A versatile data acquisition system*, Topical Wprkshop on Electronics for Particle Physics TWEPP2019, Santiago de Compostela, Spain, September 2019 (CERN, 2020)
- [3] Y. Otariid, *Pixel-Strip Modules for the CMS Tracker Phase-2 Upgrade*, Hamburg, 2023:145
- [4] T. Wilson, CERN, *Super Proton Synchrotron marks its 25th birthday* (2001)
<https://cerncourier.com/a/super-proton-synchrotron-marks-its-25th-birthday/>
- [5] CERN, *The Super Proton Synchrotron*
<https://home.cern/science/accelerators/super-proton-synchrotron>
- [6] M. Williams, S. Spannagel, J. Kroger, *Corryvreckan User Manual* (2024)